Searching for the Donor Stars of ULX Pulsars

M. Heida,[1] F.A. Harrison,[1] M. Brightman,[1] F. Fürst,[2] D. Stern,[3] and D.J. Walton[4]

[1]*Cahill Center for Astronomy and Astrophysics, California Institute of Technology, 1200 E. California Blvd, Pasadena, CA 91125, USA*
[2]*European Space Astronomy Centre (ESAC), Science Operations Department, 28692 Villanueva de la Cañada, Madrid, Spain*
[3]*Jet Propulsion Laboratory, California Institute of Technology, 4800 Oak Grove Drive, Mail Stop 169-221, Pasadena, CA 91109, USA*
[4]*Institute of Astronomy, Madingley Road, Cambridge CB3 0HA, UK*

ABSTRACT

We report on our search for the optical counterparts of two ultraluminous X-ray pulsars with known orbital periods, M82 X-2 and NGC 5907 X-1, in new and archival *HST* observations, in an effort to characterize the donor stars in these systems. We detect five near-infrared sources consistent with the position of M82 X-2 that are too bright to be single stars. We also detect seven sources in the WFC3/UVIS F336W image whose photometry matches that of $10 - 15\ M_\odot$ stars turning off the main sequence. Such stars have densities consistent with the properties of the donor star of M82 X-2 as inferred from X-ray timing analysis, although it is also possible that the donor is a lower mass star below our detection limit or that there is a significant contribution from the accretion disc to the optical emission. We detect three candidate counterparts to NGC 5907 X-1 in the near-infrared. All of these are too bright to be the donor star of the ULX, which based on its orbital period is a red giant. The high background at the location of NGC 5907 X-1 precludes us from detecting this expected donor star. The recently discovered NGC 5907 ULX-2 also falls within the field of view of the near-infrared imaging; we detect four sources in the error circle, with photometry that matches AGB stars. The star suggested to be the counterpart of NGC 5907 ULX-2 by Pintore et al. (2018) falls outside our 2-σ error circle.

Keywords: stars: neutron — X-rays: individual(M82 X-2, NGC 5907 X-1, NGC 5907 ULX-2) — infrared: stars

1. INTRODUCTION

Ultraluminous X-ray sources (ULXs) are off-nuclear point-like sources with $L_X \geq 10^{39}$ erg s^{-1}, exceeding the Eddington limit for a 10 $M_\odot$ black hole (e.g., Fabbiano 1989). Although early papers on ULXs suggested intermediate mass black holes (IMBHs; $10^2 \lesssim M_{BH} \lesssim 10^5\ M_\odot$) as the accretors in these systems (e.g. Colbert & Miller 2005), a growing body of evidence — mainly from broadband X-ray spectroscopy — favors 'stellar mass' objects exceeding the Eddington limit for the majority of sources (Gladstone et al. 2009; Sutton et al. 2013b; Walton et al. 2018). A combination of super-Eddington accretion and geometric collimation would then explain the large luminosities. This interpretation was proven to be correct for several sources by the discovery of X-ray pulsations from M82 X-2 (Bachetti

Corresponding author: M. Heida
mheida@caltech.edu

et al. 2014) and, more recently, from three other ULXs (NGC 5907 X-1, NGC 7793 P13 and SN2010da, also designated NGC 300 ULX1; Fürst et al. 2016; Israel et al. 2017a,b; Carpano et al. 2018; Binder et al. 2018), showing that in these objects the accretor is in fact a neutron star. X-ray luminosities exceeding 10^{39} erg s^{-1} have also been observed in outbursts from Be X-ray binaries with neutron star accretors (e.g. SMC X-3 and Swift J0243.6+6124, Tsygankov et al. 2017; Jaisawal et al. 2018; Wilson-Hodge et al. 2018). A fifth neutron star ULX (M51 ULX8), without X-ray pulses but identified through a cyclotron resonance feature, was reported by Brightman et al. (2018). For a recent review on ULXs we refer the reader to Kaaret et al. (2017).

Accreting magnetized neutron stars can, in principle, reach these super-Eddington luminosities through a number of mechanisms. For example, magnetic fields $\gtrsim 10^{12}$ G will collimate the accretion flow, allowing material to accrete onto the polar regions while radiation escapes from the sides of the column. Strong sur-

face magnetic fields ($\gtrsim 10^{13.5}$ G) reduce the scattering cross section for electrons, reducing the radiation pressure and increasing the effective Eddington luminosity (Basko & Sunyaev 1976; Herold 1979; Mushtukov et al. 2015). However, configurations with low magnetic fields have also been proposed (e.g. Kluzniak & Lasota 2015). All accretion theories trying to explain the seemingly super-Eddington luminosities of ULXs — with either neutron star or stellar mass black hole accretors — include a highly super-Eddington mass transfer rate from the donor star, which is difficult to reach through wind accretion. The favored scenario is therefore mass transfer through Roche lobe overflow from a massive donor star.

Very few ULX mass donor stars have been identified. The large distances to ULXs in combination with their often bright accretion discs make their donor stars hard to detect, and even more difficult to confirm spectroscopically. The only systems where spectroscopic signatures of donor stars are detected are M101 ULX1, with a Wolf-Rayet donor star (Liu et al. 2013); three ULXs (NGC 253 J004722.4-252051, NGC 925 J022721+333500 and NGC 4136 J120922+295559) with M-type supergiant donors (Heida et al. 2015, 2016); and the ULX pulsar (ULXP) NGC 7793 P13, which has a blue supergiant (B9Ia) donor (Motch et al. 2011, 2014). The recently discovered ULXP SN2010da in NGC 300 likely has a supergiant (sg) B[e] or yellow sg donor star (Lau et al. 2016; Villar et al. 2016). These are all massive stars, confirming the idea that many ULXs are an extreme class of high-mass X-ray binaries and possible progenitors of gravitational wave sources (Esposito et al. 2015; Inoue et al. 2016; Marchant et al. 2017). However, there is a significant observational bias in favor of massive companions because they are much brighter than low-mass stars. Wiktorowicz et al. (2017) predict that the majority of neutron star ULXs have low mass (≤ 1.5 $M_\odot$), red giant donors.

For ULXs with a black hole accretor, phase-resolved spectroscopic observations of the donor star are the only direct way to obtain limits on the mass of the compact object. In ULXPs we can turn this around: since neutron stars have been observed to have a very narrow range of masses ($1 - 2$ $M_\odot$, see Lattimer 2012, for a review), the mass of the compact object is known , and — unless the system is viewed at a very low inclination — we can obtain orbital parameters of the system by observing the modulation of the pulse period due to the Doppler effect. This gives us the mass function and therefore limits on the mass and average density of the donor star. In combination with direct observations of the donor it is then possible to investigate if these systems are indeed fed through Roche lobe overflow, as was recently shown for NGC 7793 P13 (Fürst et al. 2018). It is also a potential way to identify ULXs with low-mass donor stars.

In this paper we analyze new and archival *Hubble Space Telescope* (*HST*) observations of M82 X-2 and NGC 5907 X-1. We combine the photometry with orbital parameters of these systems derived from X-ray timing analyses by Bachetti et al. (2014) and Israel et al. (2017a) to put constraints on their respective donor stars. All magnitudes in this paper are Vega magnitudes.

2. DATA REDUCTION AND ANALYSIS
2.1. *HST observations*

We obtained a deep *HST* WFC3/IR F160W image of NGC 5907 (proposal ID 15074) and downloaded archival WFPC2 images of NGC 5907(Kissler-Patig et al. 1999) and WFC3 images of M82 (Lim et al. e.g. 2013; see Table 1). There are additional deep WFPC2/F606W images of NGC 5907, but NGC 5907 X-1 is just outside the field of view. The WFPC2/F450W and F814W observations of NGC 5907 have previously been analyzed by Sutton et al. (2012) who initially reported a candidate counterpart to NGC 5907 X-1 that is only detected in the F450W image ($m_{F450W} = 21.5 \pm 0.4$). However, on closer inspection, this source appeared to be spurious: it is only present in two of the three exposures with the F450W filter and likely due to cosmic rays that unfortunately hit at the same location in these two exposures (Sutton et al. 2013a). The observations of M82 were used by Voss et al. (2011) and Wang et al. (2015) to search for counterparts to M82 X-1, but not M82 X-2. Gladstone et al. (2013) did search for counterparts to M82 X-2 in older *HST* data (they call the source NGC 3034 ULX4) but they did not detect any candidate counterparts.

We use DOLPHOT version 2.0 (Dolphin 2000) for the photometric analysis. Following the DOLPHOT manuals for the WFPC2 and WFC3 modules, we photometer the *flt* (WFC3) and *c0m* (WFPC2) images separately, using the drizzled images produced by the *HST* pipeline as the reference image. The ULXs are located in crowded regions with high and variable backgrounds, especially NGC 5907 X-1. We find that setting *fitsky = 3*, with other parameter values as recommended in the manuals, yields the best results. To select good stars we filter on signal-to-noise (S/N; must be > 5), sharpness (between -0.3 and $+0.3$), object type (only stars with type 1, or 'good stars') and photometry flags (only flag values of 0 are selected).

Table 1. List of *HST* observations

Target	Prop ID	Obs date	Inst.	Filter	Exp. time (s)
NGC 5907	15074	2017-12-13	WFC3/IR	F160W	5612
	6092	1996-03-31	WFPC2	F450W	780
	6092	1996-03-31	WFPC2	F814W	480
M82	11360	2010-01-01	WFC3/UVIS	F225W	1665
	11360	2010-01-01	WFC3/UVIS	F336W	1620
	11360	2010-01-01	WFC3/IR	F110W	1195
	11360	2010-01-01	WFC3/IR	F160W	2395

2.2. *ULX positions*

We determined the positions of the ULXs and other X-ray sources in archival deep *Chandra* observations of the two galaxies (see Table 2) using the CIAO tool *wavdetect*. There are two very deep *Chandra* observations covering M82 X-2, but none of the X-ray sources have unique optical counterparts in the *HST* images. Instead we register both *Chandra* observations and the drizzled *HST* images using *Gaia* DR2 sources in the field of view. We use the CIAO tool *reproject_aspect* to register the *Chandra* observations, only considering X-ray sources with S/N > 5 (194 sources in obsid 10542 and 209 sources in obsid 10543, excluding M82 X-2 itself). There are 4 and 3 sources with matches in the *Gaia* catalog for obsid 10542 and 10543, respectively. Given the low number of sources we only calculate the x- and y-shift, leaving the rotation and scale fixed. We adopt the average residual distance between the *Gaia* and *Chandra* positions, 0.3″, as a measure of the astrometric uncertainty. The positional uncertainty due to localizing the ULX in the *Chandra* image is negligible (< 0.05″). The position of M82 X-2 in the two *Chandra* observations is consistent to within < 0.1″ — we adopt the position of the ULX in obsid 10543, RA = 09:55:51.21, Dec = +69:40:44.1 (J2000). To register the drizzled *HST* images we use the Starlink/GAIA 'fit to star positions' tool, with 21 and 19 matched sources for the IR (F160W) and UVIS (F336W) images, respectively. We adopt the rms of the fit as the final astrometric uncertainty: this is 0.12″ for the IR image and 0.04″ for the UVIS image. The uncertainty of the ULX position on the *HST* images is dominated by the uncertainty in the registration of the *Chandra* observation and is 0.3″ for both the IR and UVIS images.

For NGC 5907 we retrieved two *Chandra* observations from the archive. The shorter one (obsid 12987) contains NGC 5907 X-1 but no X-ray sources that can be used for cross-matching with the *HST* image or other optical catalogs. The longer observation (obsid 20830) is a recent DDT observation obtained while NGC 5907 X-1 was in an off-state (Pintore et al. 2018; a previous off-state of this source was observed by Walton et al. 2015). This observation does contain two X-ray sources with unique counterparts in our WFC3/IR image. Using *reproject_aspect*, we first register the short *Chandra* observation to the longer one using 8 common X-ray sources with S/N > 4. The average residual after the shift is 0.23″. We then use the two overlapping sources between the longer *Chandra* observation and our WFC3/IR image to register the *Chandra* observations to the *HST* image. With only two sources we cannot calculate the uncertainty in this step; we conservatively assume an error of 0.3″. Quadratically adding the two uncertainties gives a total astrometric uncertainty of 0.4″ (again, the error in the localization of the ULX in the *Chandra* image is negligible). The position of the ULXP on the WFC3 image is RA = 15:15:58.66, Dec = +56:18:10.3 (J2000).

The new ULX reported by Pintore et al. (2018, NGC 5907 ULX-2) is visible in *Chandra* observation 20830. Its position in our WFC3 F160W image is RA = 15:16:01.13, Dec. = +56:17:51.5 (J2000), with an astrometric uncertainty of 0.3″ that is mainly due to the registration of *Chandra* observation 20830 to our *HST* image.

2.3. *Limiting magnitudes*

The limiting magnitudes of the *HST* observations vary across the images due to the local background. We use the DOLPHOT *fakestar* routine to determine the limiting magnitudes at the positions of the ULXs. In every image we insert 2000 fake stars distributed normally around the position of the ULX, spanning a range of 8 input magnitudes. We then run DOLPHOT in fakestar mode to obtain the photometry of these fake stars. We adopt as the limiting magnitude the faintest magnitude at which ≥ 90% of the fake stars are retrieved with S/N ≥ 5. To make sure our photometry is accurate, we also check that the retrieved magnitudes of the fake stars are con-

Table 2. List of *Chandra* observations

Target	Obs ID	Obs start date	Inst.	Exp. time (ks)
NGC 5907	12987	2012-02-11	ACIS-S	16.0
	20830	2017-11-07	ACIS-S	51.3
M82	10542	2009-06-24	ACIS-S	118.6
	10543	2009-07-01	ACIS-S	118.5

Table 3. Limiting magnitudes of *HST* images at the position of the ULXs

Source	*HST* filter	Limiting magnitude
M82 X-2	F225W	25.1
	F336W	26.4
	F110W	18.8
	F160W	18.8
NGC 5907 X-1	F450W	25.5
	F814W	23.6
	F160W	22.0
NGC 5907 ULX-2	F450W	25.8
	F814W	25.0
	F160W	23.7

Table 4. DOLPHOT magnitudes of sources labeled in Figure 1. Listed magnitudes are not corrected for extinction

Source	m_{F160W}	m_{F814W}	m_{F450W}
NGC 5907 X-1			
1	21.61 ± 0.01	23.53 ± 0.14	25.0 ± 0.2
2	21.75 ± 0.01	> 23.6	> 25.5
3	21.91 ± 0.02	> 23.6	> 25.5
NGC 5907 ULX-2			
1	22.68 ± 0.02	> 25.0	24.7 ± 0.3
2	22.73 ± 0.02	> 25.0	> 25.8
3	23.21 ± 0.03	> 25.0	> 25.8
4	23.38 ± 0.04	> 25.0	> 25.8

sistent with their input magnitudes to within 0.3 mag. In two cases (the WFC3/F160W and WFPC2/F814W observations of NGC 5907 X-1) we find that the retrieved magnitudes diverge significantly from the input magnitudes. This is likely due to imperfect modeling of the complex background by DOLPHOT. In these two cases we adopt the faintest magnitude at which $\geq 90\%$ of the fake stars are retrieved within 0.3 mag from their input magnitude as our limiting magnitude. All magnitude limits are listed in Table 3; we only consider sources brighter than this limit in our analysis.

3. RESULTS

3.1. *NGC 5907*

We detect three sources brighter than the limiting magnitude inside the 2-σ error circle of NGC 5907 X-1 in our F160W image (see center right panel in Figure 1 and Table 4). The errors listed are the statistical errors as calculated by DOLPHOT. The brightest source is also detected in the F814W and F450W images, at $m_{\mathrm{F814W}} \approx 23.5$ and $m_{\mathrm{F450W}} \approx 25.0$. No other point sources are detected in the F450W and F814W images.

We detect four sources brighter than the limiting magnitude in the 2-σ error circle of NGC 5907 ULX-2 in our F160W image (see right-hand panel in Figure 1 and Ta-

ble 4). Only the brightest of these sources is detected in the F450W image. No sources are significantly detected in the F814W image. The Pintore et al. (2018) preferred counterpart is visible in our F160W and F814W images (indicated with a magenta circle in Figure 1), but its position is inconsistent (at > 3-σ) with our localization of the ULX. This is due to our smaller localization uncertainty: our $1 - \sigma$ uncertainty is $0.3''$ versus $0.42''$ for Pintore et al. (2018), as they used a different method to register the *Chandra* and *HST* images.

3.2. *M82 X-2*

We detect five sources in the 2-σ error circle of M82 X-2 in the NIR images, with $17.4 \leq m_{F110W} \leq 18.4$ and $16.0 \leq m_{F160W} \leq 16.8$ (see right-hand panel in Figure 2 and Table 5). Two of these, as well as seven additional sources that are not detected in the NIR images, are detected in the F336W image (center panel in Figure 2). No point sources are significantly detected in the F225W image.

4. DISCUSSION

We searched for counterparts to two ULXPs in new and archival *HST* observations. Both sources are located in crowded regions with high extinction — M82 X-2 in the center of M82, and NGC 5907 X-1 in the dust
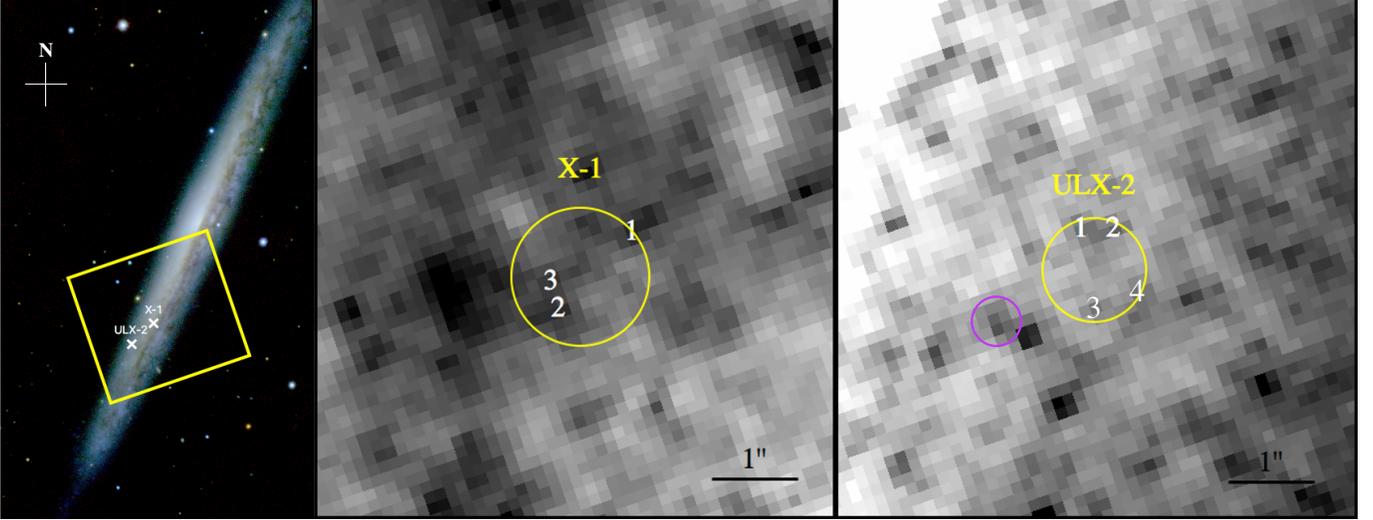
Figure 1. *Left:* False-color PanSTARRS image of NGC 5907 (*g'*, *i'* and *y'* bands) with the locations of the two ULXs marked with white crosses. The yellow box indicates the field of view of our WFC3/F160W observation. *Middle and right:* The locations of the two ULXs on our WFC3/F160W observations. The yellow circles indicate the 2-σ regions around the X-ray positions of the ULXs. The retrieved magnitudes of the sources labeled in this Figure are listed in Table 4. The counterpart to NGC 5907 ULX-2 proposed by Pintore et al. (2018) is indicated with a magenta circle.
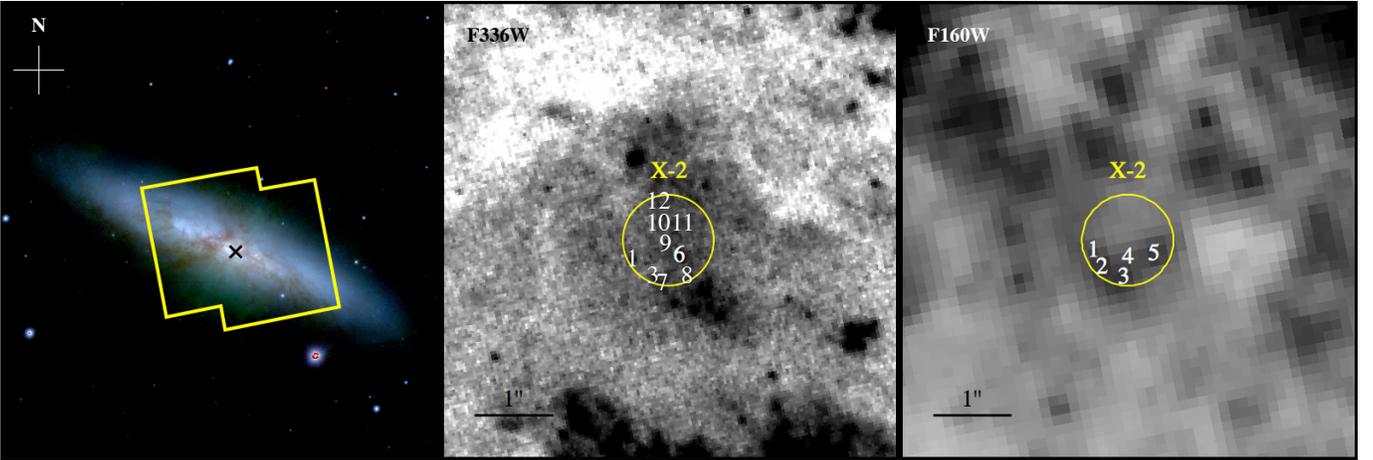
Figure 2. *Left:* False-color PanSTARRS image of M82 (*g'*, *r'* and *y'* bands) with the location of M82 X-2 marked with a black cross. The yellow box indicates the field of view of the archival WFC3/NIR observations. The field of view of the WFC3/UVIS observations is similar. *Middle and right:* The location of M82 X-2 on the WFC3/F336W (middle) and WFC3/F160W (right) observations. The yellow circles indicate the 2-σ region around the X-ray position of the ULX. The retrieved magnitudes of the sources labeled in this Figure are listed in Table 5.

lane of the edge-on spiral galaxy NGC 5907. We detect multiple potential counterparts to both ULXPs as well as to a second, recently discovered ULX in NGC 5907. Given the distance modulus to NGC 5907 ($m - M = 31.17 \pm 0.09$, corresponding to a distance of 17.1 Mpc; Tully et al. 2013), the absolute magnitudes of the counterparts to NGC 5907 X-1 in the F160W filter are $-9.5 \leq M_{F160W} \leq -9.3$. Counterpart 1 is also detected in the F450W and F814W filters with absolute magnitudes of $M_{F814W} \approx -7.6$ and $M_{F450W} \approx -6.0$, while the other two counterparts are fainter than -7.6

mag in the F814W filter and -5.7 mag in the F450W filter, respectively. The counterparts to NGC 5907 ULX-2 have $-8.5 \leq M_{F160W} \leq -7.8$. Counterpart 1 is also detected in the F450W filter with absolute magnitude $M_{F450W} \approx -6.5$; the other counterparts are fainter than -5.4 mag in the F450W filter and all counterparts are fainter than -6.2 mag in the F814W filter.

The five counterparts of M82 X-2 (with a distance modulus of 27.74 ± 0.08, corresponding to a distance of 3.5 Mpc; Tully et al. 2013) that are detected in the near-IR images have absolute magnitudes $-11.7 \leq$

Table 5. DOLPHOT magnitudes of sources labeled in Figure 2. Listed magnitudes are not corrected for extinction

Source	m_{F160W}	m_{110W}	m_{F336W}	m_{F225W}
M82 X-2				
1	16.719 ± 0.001	18.411 ± 0.002	24.9 ± 0.1	> 25.1
2	16.006 ± 0.001	17.386 ± 0.001	> 26.4	> 25.1
3	16.153 ± 0.001	17.537 ± 0.001	25.3 ± 0.2	> 25.1
4	16.822 ± 0.002	18.442 ± 0.002	> 26.4	> 25.1
5	16.046 ± 0.001	17.436 ± 0.001	> 26.4	> 25.1
6	> 18.8	> 18.8	24.39 ± 0.09	> 25.1
7	> 18.8	> 18.8	25.4 ± 0.2	> 25.1
8	> 18.8	> 18.8	25.3 ± 0.2	> 25.1
9	> 18.8	> 18.8	25.6 ± 0.2	> 25.1
10	> 18.8	> 18.8	25.6 ± 0.2	> 25.1
11	> 18.8	> 18.8	25.9 ± 0.3	> 25.1
12	> 18.8	> 18.8	25.7 ± 0.3	> 25.1

$M_{F160W} \leq -10.9$ and $-10.4 \leq M_{F110W} \leq -9.2$. Counterparts 1 and 3 are also detected in the F336W image with $M_{F336W} \approx -2.8$ and -2.4, respectively, while the other three are fainter than -1.3 mag in that band. The other seven counterparts are only detected in the F336W image, with $-3.4 \leq M_{F336W} \leq -1.8$. They are fainter than -8.9 mag in both the F110W and F160W bands. All counterparts are fainter than -2.6 mag in the F225W band.

4.1. Reddening

The foreground Galactic extinction in the direction of NGC 5907 is negligible ($A_V \approx 0.03$, Schlegel et al. 1998). However, NGC 5907 X-1 is located on the dust lane of this edge-on spiral (see Fig. 1) and the extinction due to dust and gas in the galaxy itself is significant. The hydrogen column density as measured in the X-ray spectra is $N_{\mathrm{H}} = 0.4 - 0.9 \times 10^{22}$ cm^{-2} (Sutton et al. 2013b; Walton et al. 2015; Fürst et al. 2017). This translates into a V-band absorption $A_V \approx 1.8 - 4.1$ (Güver & Özel 2009). It is not clear from the X-ray observations whether the absorption is variable or not (Fürst et al. 2017). If it is variable, part of this X-ray absorbing material is likely local to the system itself and may not obscure the companion star, and A_V is likely closer to the lower end of this range.

NGC 5907 ULX-2 is located further away from the central dust lane; Pintore et al. (2018) found no local extinction on top of the foreground Galactic absorption from their analysis of the X-ray spectrum of this source.

The foreground Galactic extinction in the direction of M82 is $A_V = 0.485$ (Schlegel et al. 1998). On top of that there is significant extinction due to gas and dust ($A_V \geq 1.55$) in the core of the galaxy, where M82 X-2 is located (Hutton et al. 2014).

4.2. Limits on donor star properties from X-ray timing

Assuming circular orbits and accretion via Roche lobe overflow, the density of the donor star can be determined directly given the orbital period of the binary system and the mass of the accretor, using the equation for the Roche radius (Eggleton 1983) and Kepler's laws. For M82 X-2, the orbital period was reported by Bachetti et al. (2014) as 2.53260 ± 0.00005 days, with an eccentricity $\epsilon < 0.003$ and a projected semi-major axis ($a \sin(i)$) of 22.225 ± 0.004 ls.

For NGC 5907 X-1 these values are not as well constrained. Israel et al. (2017a) performed a likelihood analysis to obtain the orbital parameters of the system (their Figure 2). They found a most-probable period $P_{\mathrm{orb}} = 5.3^{+2.0}_{-0.9}$ days with $a \sin(i) = 2.5^{+4.3}_{-0.8}$ ls.

For M82 X-2, the lower limit on the donor star mass is ~ 5 $M_\odot$, assuming a neutron star mass of 1.4 $M_\odot$ and a system inclination $\leq 60°$ (Bachetti et al. 2014). For NGC 5907 X-1, the mass function for the most likely parameters reported by Israel et al. (2017a) is 6×10^{-4} $M_\odot$, implying a lower limit for the donor star of ~ 0.1 $M_\odot$. The measurements of Israel et al. (2017a) also allow for a longer orbital period (up to ~ 21 days) with a larger projected semi-major axis, that would imply a higher minimum mass for the donor star (e.g. 29 $M_\odot$ for an orbital period of 18 days and $a \sin(i) = 200$ ls).

We plot the relation between allowed masses and radii for M82 X-2 and NGC 5907 X-1 in Figure 3. For comparison, we also show the relation for NGC 7793 P13, a ULXP with a blue supergiant companion with a mass of 18 – 23 $M_\odot$ and a radius of 96 – 125 $R_\odot$ (Motch et al. 2014; Fürst et al. 2018). In the background we show evolution tracks of single, non-rotating stars at solar metallicity from the MESA Isochrones and Stellar Tracks (MIST) project (Choi et al. 2016; Dotter 2016). The donor stars in ULXPs obviously do not evolve in isolation, which will impact their evolution tracks (see e.g. Rappaport et al. 2005; Patruno & Zampieri 2008, 2010; Ambrosi & Zampieri 2018). However, comparing the possible masses and radii of the ULXP donors with those of single stars is useful to show the most plausible evolutionary stage of the donor stars in these systems.

From Figure 3 we can see that the donor star of M82 X-2 is most likely just turning off the main sequence (as was also shown by Fragos et al. 2015), while the donor of NGC 5907 X-1should be a more evolved star in the Hertzsprung gap or on the red giant branch.
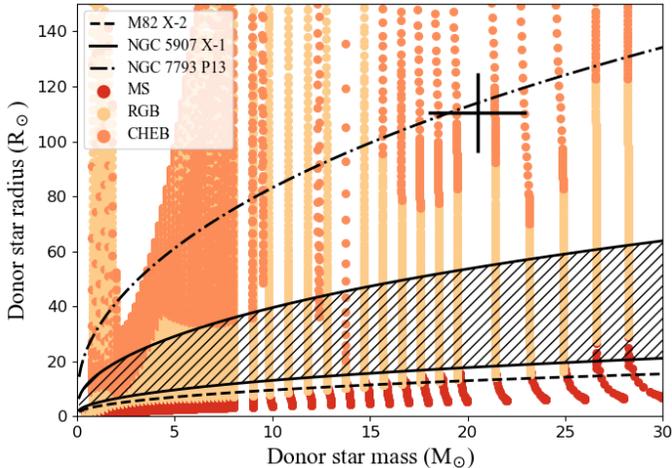
Figure 3. Acceptable values of masses and radii of the donor stars of three ULXPs based on their orbital periods, assuming they accrete through Roche-lobe overflow. The lines plotted here assume a neutron star mass of 1.4 $M_\odot$, but are essentially the same for a neutron star mass of 2 $M_\odot$. The shaded region indicates the range of allowed orbital periods for NGC 5907 X-1 (4 - 21 days). The black cross indicates the mass and radius of the donor star of NGC 7793 P13 (Motch et al. 2014; Fürst et al. 2018). In the background are plotted evolution tracks of single stars at solar metallicity obtained from the MIST project. The evolutionary stages plotted here are main sequence (MS), red giant branch including the Hertzsprung gap (RGB) and core helium burning (CHEB).

4.3. *Contribution from the accretion disc*

The colors and magnitudes of the optical counterparts of ULXs can be significantly affected by irradiation of the donor star and emission from the (supercritical) accretion disc (see e.g. Copperwheat et al. 2005, 2007; Patruno & Zampieri 2008, 2010; Ambrosi & Zampieri 2018 for theoretical work, and Roberts et al. 2011; Grisé et al. 2012 for observations). The theoretical work has so far mostly focused on systems with a (massive) black hole as the accretor, and shows larger effects for more massive black holes; the impact on the optical counterparts of neutron star ULXs may be less pronounced. For example, the optical counterpart of NGC 7793 P13 is affected by irradiation of the donor star, resulting in an observed spectral type that changes with the orbital phase of the system. However, its supergiant donor completely dominates the optical emission and there does not appear to be a significant contribution from an accretion disc to the optical light (Motch et al. 2014). Simulations like those of Ambrosi & Zampieri (2018) for systems with a neutron star accretor would be very useful in assessing the effect of irradiation and the accretion disc on the optical/near-IR emission for ULXPs with non-

supergiant donors. In the following we assume that the optical/near-IR emission from the ULXPs is dominated by the donor star as is the case for NGC 7793 P13.

4.4. *Limits on donor star properties from photometry*

To check if the sources we detect in the *HST* images could be the donor stars of these ULXPs we downloaded synthetic WFC3 and WFPC2 photometry files at solar metallicity with $A_V = 1.8$ and 4.1 (for NGC 5907 X-1) and at [Fe/H] = -0.25 (Nagao et al. 2011) and $A_V = 2.0$ (for M82 X-2) from the MIST website, as well as WFC3 and WFPC2 photometry at solar metallicity with $A_V = 0.03$ for NGC 5907 ULX-2. In the case of NGC 5907 X-1, all stars with magnitudes consistent with the observed ones are red supergiant stars with radii larger than 400 $R_\odot$— none of these can be the stellar companion to the ULXP. The limiting magnitude of our WFC3/F160W image is too bright to detect the donor star, due to the high background in this region. The F160W magnitudes and F450W and F814W limits of the sources detected in the error circle of NGC 5907 ULX-2 are consistent with asymptotic giant branch (AGB) stars. Without information on the orbital period and accretor mass in this system, we cannot say anything about the likelihood that one of these sources is the donor star to the ULX.

The near-IR counterparts to M82 X-2 are even brighter, and no single star in the MIST simulations matches these F110W and F160W absolute magnitudes. These sources may be compact star clusters — the resolution of the WFC3/IR camera at $1.6\mu m$ corresponds to ~ 3 pc at the distance of M82. The magnitudes and limits of sources that are only detected in the WFC3/UVIS F336W image do match those of single stars with masses and radii consistent with a possible donor of M82 X-2: $10 - 15$ $M_\odot$ stars just turning off the main sequence. One of these counterparts could potentially be the donor star of M82 X-2, although it is also possible that the donor is a lower mass star too faint to be detected in the F336W image. In addition, one of these sources may be the real counterpart, but dominated by irradiation and/or emission from the accretion disc.

5. CONCLUSIONS

We obtained new WFC3/NIR images of NGC 5907 and used those in conjunction with deep archival WFPC2 images to search for the donor star of NGC 5907 X-1. The sources we detect are too bright to be the donor star of the ULXP, which based on its orbital period should be a red giant (see Figure 3). The high background at the location of NGC 5907 X-1 precludes us from detecting the expected donor star, assuming that the donor dominates the optical/near-IR emission from the system. The recently discovered

NGC 5907 ULX-2 also falls within the field of view; we detect four sources in the error circle, with photometry that matches AGB stars. The star suggested to be the counterpart by Pintore et al. (2018) falls outside our 2-σ error circle.

We also retrieved deep WFC3/NIR and WFC3/UVIS images of M82 X-2 from the *HST* archive to search for the donor star of this ULXP. The sources detected in the NIR images are too bright to be single stars, but we also detect several sources in the UVIS F336W image whose photometry matches that of $10 - 15\ M_\odot$ stars turning off the main sequence. Such stars have densities consistent with the donor star of M82 X-2, although it is also possible that the donor is a lower mass star fainter than our detection limit or that the optical light is dominated by irradiation and/or emission from the accretion disc.

Characterizing the donor stars of ULXPs is important for testing models of binary evolution. To date, the only system with a spectroscopically characterized donor star is NGC 7793 P13, which hosts a blue supergiant star (Motch et al. 2011, 2014). However, the majority of ULXPs are expected to have lower mass red giant donor stars (Wiktorowicz et al. 2017). Shorter period systems such as M82 X-2 and NGC 5907 X-1 may be examples of such lower mass systems, but the crowded environments and the large distances to these sources make direct detection and especially spectroscopic characterization unfeasible with currently available instruments. For the nearest ULXs this may change when the first 30-40 m class telescopes become operational.

Facilities: HST (WFPC2 and WFC3), Chandra (ACIS), Gaia

Software: astropy (Astropy Collaboration et al. 2013), DOLPHOT (Dolphin 2000), MESA (Paxton et al. 2011, 2013, 2015), CIAO (Fruscione et al. 2006)

REFERENCES

Ambrosi, E., & Zampieri, L. 2018, MNRAS, 480, 4918, doi: 10.1093/mnras/sty2213

Astropy Collaboration, Robitaille, T. P., Tollerud, E. J., et al. 2013, A&A, 558, A33, doi: 10.1051/0004-6361/201322068

Bachetti, M., Harrison, F. A., Walton, D. J., et al. 2014, Nature, 514, 202, doi: 10.1038/nature13791

Basko, M. M., & Sunyaev, R. A. 1976, MNRAS, 175, 395, doi: 10.1093/mnras/175.2.395

Binder, B., Levesque, E. M., & Dorn-Wallenstein, T. 2018, ApJ, 863, 141, doi: 10.3847/1538-4357/aad3bd

Brightman, M., Harrison, F. A., Fürst, F., et al. 2018, Nature Astronomy, 2, 312, doi: 10.1038/s41550-018-0391-6

Carpano, S., Haberl, F., Maitra, C., & Vasilopoulos, G. 2018, MNRAS, 476, L45, doi: 10.1093/mnrasl/sly030

Choi, J., Dotter, A., Conroy, C., et al. 2016, ApJ, 823, 102, doi: 10.3847/0004-637X/823/2/102

Colbert, E. J. M., & Miller, M. C. 2005, in The Tenth Marcel Grossmann Meeting. On recent developments in theoretical and experimental general relativity, gravitation and relativistic field theories, ed. M. Novello, S. Perez Bergliaffa, & R. Ruffini, 530–+

Copperwheat, C., Cropper, M., Soria, R., & Wu, K. 2005, MNRAS, 362, 79, doi: 10.1111/j.1365-2966.2005.09223.x

—. 2007, MNRAS, 376, 1407, doi: 10.1111/j.1365-2966.2007.11551.x

Dolphin, A. E. 2000, PASP, 112, 1383, doi: 10.1086/316630

Dotter, A. 2016, ApJS, 222, 8, doi: 10.3847/0067-0049/222/1/8

Eggleton, P. P. 1983, ApJ, 268, 368, doi: 10.1086/160960

Esposito, P., Israel, G. L., Milisavljevic, D., et al. 2015, MNRAS, 452, 1112, doi: 10.1093/mnras/stv1379

Fabbiano, G. 1989, ARA&A, 27, 87, doi: 10.1146/annurev.aa.27.090189.000511

Fragos, T., Linden, T., Kalogera, V., & Sklias, P. 2015, ApJ, 802, L5, doi: 10.1088/2041-8205/802/1/L5

Fruscione, A., McDowell, J. C., Allen, G. E., et al. 2006, in Society of Photo-Optical Instrumentation Engineers (SPIE) Conference Series, Vol. 6270, Society of Photo-Optical Instrumentation Engineers (SPIE) Conference Series

Fürst, F., Walton, D. J., Stern, D., et al. 2017, ApJ, 834, 77, doi: 10.3847/1538-4357/834/1/77

Fürst, F., Walton, D. J., Harrison, F. A., et al. 2016, ApJL, 831, L14, doi: 10.3847/2041-8205/831/2/L14

Fürst, F., Walton, D. J., Heida, M., et al. 2018, A&A, 616, A186, doi: 10.1051/0004-6361/201833292

Gladstone, J. C., Copperwheat, C., Heinke, C. O., et al. 2013, ApJS, 206, 14, doi: 10.1088/0067-0049/206/2/14

Gladstone, J. C., Roberts, T. P., & Done, C. 2009, MNRAS, 397, 1836, doi: 10.1111/j.1365-2966.2009.15123.x

Grisé, F., Kaaret, P., Corbel, S., et al. 2012, ApJ, 745, 123, doi: 10.1088/0004-637X/745/2/123

Güver, T., & Özel, F. 2009, MNRAS, 400, 2050, doi: 10.1111/j.1365-2966.2009.15598.x

Heida, M., Jonker, P. G., Torres, M. A. P., et al. 2016, MNRAS, 459, 771, doi: 10.1093/mnras/stw695

Heida, M., Torres, M. A. P., Jonker, P. G., et al. 2015, MNRAS, 453, 3510, doi: 10.1093/mnras/stv1853

Herold, H. 1979, PhRvD, 19, 2868, doi: 10.1103/PhysRevD.19.2868

Hutton, S., Ferreras, I., Wu, K., et al. 2014, MNRAS, 440, 150, doi: 10.1093/mnras/stu185

Inoue, Y., Tanaka, Y. T., & Isobe, N. 2016, MNRAS, 461, 4329, doi: 10.1093/mnras/stw1637

Israel, G. L., Belfiore, A., Stella, L., et al. 2017a, Science, 355, 817, doi: 10.1126/science.aai8635

Israel, G. L., Papitto, A., Esposito, P., et al. 2017b, MNRAS, 466, L48, doi: 10.1093/mnrasl/slw218

Jaisawal, G. K., Naik, S., & Chenevez, J. 2018, MNRAS, 474, 4432, doi: 10.1093/mnras/stx3082

Kaaret, P., Feng, H., & Roberts, T. P. 2017, ARA&A, 55, 303, doi: 10.1146/annurev-astro-091916-055259

Kissler-Patig, M., Ashman, K. M., Zepf, S. E., & Freeman, K. C. 1999, AJ, 118, 197, doi: 10.1086/300919

Kluzniak, W., & Lasota, J. P. 2015, MNRAS, 448, L43, doi: 10.1093/mnrasl/slu200

Lattimer, J. M. 2012, Annual Review of Nuclear and Particle Science, 62, 485, doi: 10.1146/annurev-nucl-102711-095018

Lau, R. M., Kasliwal, M. M., Bond, H. E., et al. 2016, ApJ, 830, 142, doi: 10.3847/0004-637X/830/2/142

Lim, S., Hwang, N., & Lee, M. G. 2013, ApJ, 766, 20, doi: 10.1088/0004-637X/766/1/20

Liu, J.-F., Bregman, J. N., Bai, Y., Justham, S., & Crowther, P. 2013, Nature, 503, 500, doi: 10.1038/nature12762

Marchant, P., Langer, N., Podsiadlowski, P., et al. 2017, A&A, 604, A55, doi: 10.1051/0004-6361/201630188

Motch, C., Pakull, M. W., Grisé, F., & Soria, R. 2011, Astronomische Nachrichten, 332, 367, doi: 10.1002/asna.201011501

Motch, C., Pakull, M. W., Soria, R., Grisé, F., & Pietrzyński, G. 2014, Nature, 514, 198, doi: 10.1038/nature13730

Mushtukov, A. A., Suleimanov, V. F., Tsygankov, S. S., & Poutanen, J. 2015, MNRAS, 454, 2539, doi: 10.1093/mnras/stv2087

Nagao, T., Maiolino, R., Marconi, A., & Matsuhara, H. 2011, A&A, 526, A149, doi: 10.1051/0004-6361/201015471

Patruno, A., & Zampieri, L. 2008, MNRAS, 386, 543, doi: 10.1111/j.1365-2966.2008.13063.x

—. 2010, MNRAS, 403, L69, doi: 10.1111/j.1745-3933.2010.00817.x

Paxton, B., Bildsten, L., Dotter, A., et al. 2011, ApJS, 192, 3, doi: 10.1088/0067-0049/192/1/3

Paxton, B., Cantiello, M., Arras, P., et al. 2013, ApJS, 208, 4, doi: 10.1088/0067-0049/208/1/4

Paxton, B., Marchant, P., Schwab, J., et al. 2015, ApJS, 220, 15, doi: 10.1088/0067-0049/220/1/15

Pintore, F., Belfiore, A., Novara, G., et al. 2018, MNRAS, 477, L90, doi: 10.1093/mnrasl/sly048

Rappaport, S. A., Podsiadlowski, P., & Pfahl, E. 2005, MNRAS, 356, 401, doi: 10.1111/j.1365-2966.2004.08489.x

Roberts, T. P., Gladstone, J. C., Goulding, A. D., et al. 2011, Astronomische Nachrichten, 332, 398, doi: 10.1002/asna.201011508

Schlegel, D. J., Finkbeiner, D. P., & Davis, M. 1998, ApJ, 500, 525, doi: 10.1086/305772

Sutton, A. D., Roberts, T. P., Gladstone, J. C., et al. 2013a, MNRAS, 434, 1702, doi: 10.1093/mnras/stt1133

Sutton, A. D., Roberts, T. P., & Middleton, M. J. 2013b, MNRAS, 435, 1758, doi: 10.1093/mnras/stt1419

Sutton, A. D., Roberts, T. P., Walton, D. J., Gladstone, J. C., & Scott, A. E. 2012, MNRAS, 423, 1154, doi: 10.1111/j.1365-2966.2012.20944.x

Tsygankov, S. S., Doroshenko, V., Lutovinov, A. A., Mushtukov, A. A., & Poutanen, J. 2017, A&A, 605, A39, doi: 10.1051/0004-6361/201730553

Tully, R. B., Courtois, H. M., Dolphin, A. E., et al. 2013, AJ, 146, 86, doi: 10.1088/0004-6256/146/4/86

Villar, V. A., Berger, E., Chornock, R., et al. 2016, ApJ, 830, 11, doi: 10.3847/0004-637X/830/1/11

Voss, R., Nielsen, M. T. B., Nelemans, G., Fraser, M., & Smartt, S. J. 2011, MNRAS, 418, L124, doi: 10.1111/j.1745-3933.2011.01157.x

Walton, D. J., Harrison, F. A., Bachetti, M., et al. 2015, ApJ, 799, 122, doi: 10.1088/0004-637X/799/2/122

Walton, D. J., Fürst, F., Heida, M., et al. 2018, ApJ, 856, 128, doi: 10.3847/1538-4357/aab610

Wang, S., Liu, J., Bai, Y., & Guo, J. 2015, ApJL, 812, L34, doi: 10.1088/2041-8205/812/2/L34

Wiktorowicz, G., Sobolewska, M., Lasota, J.-P., & Belczynski, K. 2017, ApJ, 846, 17, doi: 10.3847/1538-4357/aa821d

Wilson-Hodge, C. A., Malacaria, C., Jenke, P. A., et al. 2018, ApJ, 863, 9, doi: 10.3847/1538-4357/aace60